Experimental Thermal and Fluid Science 62 (2015) 85–98

Contents lists available at ScienceDirect

Experimental Thermal and Fluid Science

journal homepage: www.elsevier.com/locate/etfs

Interfacial waves in stratified viscous oil–water flow

Marcelo S. de Castro [a,*], Oscar M.H. Rodriguez [b]

[a] Department of Energy, Faculty of Mechanical Engineering, University of Campinas (UNICAMP), Av. Mendeleyev, 200, 13083-860 Campinas, SP, Brazil
[b] Department of Mechanical Engineering, Sao Carlos School of Engineering, University of Sao Paulo (USP), Av. Trabalhador São Carlense, 400, 13566-970 Sao Carlos, SP, Brazil

ARTICLE INFO

Article history:
Received 8 October 2014
Accepted 3 December 2014
Available online 12 December 2014

Keywords:
Liquid–liquid flow
Oil–water flow
Stratified flow pattern
Interfacial wave structure
Experiments
Wave geometry
Correlation

ABSTRACT

The analysis of the interfacial wave properties is an important point in understanding of many aspects of separated-flow patterns (annular and stratified). One may cite flow pattern stability, pressure drop and heat transfer as characteristics affected by the wave properties. Previous studies have shown that the phenomenon of flow pattern transition in stratified flow can be related to the interfacial wave structure (problem of hydrodynamic instability). The study of the wavy stratified flow pattern requires the characterization of the interface, *i.e.*, average wave shape, wave speed, amplitude and wavelength as a function of flow properties. Studies on waves in stratified liquid–liquid flow are scanty, even more when related to viscous oils. This article offers new experimental data on interfacial waves collected in a glass test line of 12 m and 0.026 m i.d., oil (density and viscosity of 854 kg/m^3 and 0.3 Pa s at 20 °C, respectively) and tap water as the working fluids; the stratified flow was filmed with a high speed video camera at several inclinations from horizontal (−5°, 0°, 5°, 10°). New experimental data and available literature data of interfacial waves in oil–water flow were collected, analyzed and correlated to the flow properties by dimensionless numbers of Reynolds, Froude and Weber. A second-order Fourier series is proposed to model the wave shape. The correlations can be used to predict the average wave geometry and wave speed of typical oil–water interfacial waves within a significant range of superficial velocities and pipe inclinations. Considering the simplicity of the proposed correlation, the agreement between data and predicted wave is encouraging.

1. Introduction

In industrial processes the presence of multiphase flows is very common. In multiphase flows, the way that the immiscible phases are geometrically arranged in a pipe, *i.e.* the flow pattern, is important in defining the way that each flow should be modeled. For example, dispersion should be analyzed by the homogeneous model, vertical slug flow by the drift flux model and stratified and annular flows via the separated flow model. If the longitudinal dimension of a pipe is relatively larger than the others the one-dimensional approach is usually applicable. Important characteristics of flow, as pressure drop, heat transfer, corrosion and structural vibration, are examples of topics that depend on the geometrical configuration of the immiscible phases, or flow patterns [1]. The interest in liquid–liquid flow has increased since offshore oil production is on the rise over the last years, although investigations on such flows are not as common as those on gas–liquid flow. The stratified liquid–liquid flow is present in directional oil wells and pipelines and is characterized by the heavier and lighter phases located at the bottom and top part of the pipe, respectively, divided by an interface that can be smooth, wavy or present droplets of one phase into the other. The understanding and characterization of the interfacial wavy structure allow for the correct modeling of the flow; as already pointed out by Wallis [2] and his equivalent-sand-roughness concept for annular gas–liquid flow. Recently, it was extended to stratified liquid–liquid flow by Rodriguez and Baldani [3]. According to those authors the wavy structure impacts on the interfacial friction factor and, consequently, on the pressure drop and in-situ holdup predictions.

The interfacial-wavy structure was studied in gas–liquid flow by Bontozoglou and Hanratty [4] and Bontozoglou [5]. One of the findings was that the two-phase friction factor of wavy stratified flow can be about fifty times as high as the friction factor of smooth stratified flow. Li et al. [6] also studied the gas–liquid stratified flow pattern and showed that the interfacial waves have significant influence on heat transfer and pressure drop. The interfacial wavy structure of separated flows in gas–liquid systems and its influence on the flow have been further studied by a few researches [7]. The effect of interfacial waves on the friction factor with or without gravity in annular flow, the role played by stratified-flow parameters on slug flow formation and a numerical solution for stratified

* Corresponding author. Tel.: +55 19 35213264; fax: +55 19 32893722.
E-mail address: mcastro@fem.unicamp.br (Marcelo S. de Castro).

http://dx.doi.org/10.1016/j.expthermflusci.2014.12.003
0894-1777/

Nomenclature

Uws	water superficial velocity, m/s
Uos	oil superficial velocity, m/s
V_w	water *in-situ* velocity, m/s
V_o	oil *in-situ* velocity, m/s
D	pipe's internal diameter, m
Dh	hydraulic diameter, m
g	gravitational acceleration, m/s^2
Froude (Fr^*)	modified two-phase Froude number, dimensionless
Weber (We^*)	modified two-phase Weber number, dimensionless
Reynolds (*Re*)	Reynolds number, dimensionless
c	wave's speed, m/s
y	ordinate, mm
x	abscissa, mm
QCV	quick-closing-valves technique
h_w	water height
S	standard deviation

Greek

θ	inclination of the pipeline, rad
ε	volumetric fraction, dimensionless
α	wave amplitude, mm
λ	wavelength, mm
σ	interfacial tension, N/m

Subscript

w	water-phase
o	oil-phase
m	mean
α	relative to the wave amplitude
λ	relative to the wavelength
c	relative to the wave speed

Superscript

*	normalized coordinates

flow that considers an effective roughness due to the waves have been the research subject of, respectively, Wang et al. [8,9], Dyment and Boudlal [10] and Berthelsen and Ytrehus [11]. Also, Andritsos and Hanratty [12,13] and Andritsos [14] had the interfacial wave in horizontal gas–liquid stratified (water and glycerin) flows as subject of research. Those authors measured the interfacial wave amplitude and speed via conductive probes; they found that the interfacial friction factor increases rapidly with the rise of high amplitude interfacial waves. In flows with low viscosity liquids the wave amplitude increases and the wavelength decreases with the increase of the gas flow rate; with high viscous liquids the increase in the gas flow rate make the wave crest curved.

The wavy stratified flow in liquid–liquid flows was experimentally observed by Chakrabarti et al. [15,16] using water and kerosene as working fluids. Accordingly to Charles and Lilleleht [17] the rise of waves in co-current liquid–liquid flows is related to the transition from laminar to turbulent of the less viscous phase. In the case of viscous oil–water stratified flow, Castro et al. [18] found that the wave characteristics might be related to a modified Froude number. Sotgia et al. [19] affirmed that the wavelength of the interfacial wave in viscous oil water-flow decrease as the water superficial velocity decreases. Yusuf et al. [20] studied the effect of the oil viscosity in flow pattern classification, pressure gradient and phase inversion in oil–water flows by comparing their results with other from literature. They observed that the interfacial wave amplitude increase with increasing the water superficial velocity.

Looking at the cross-sectional interface shape, Brauner et al. [21] compared the gas–liquid and liquid–liquid interfaces in stratified flow. In the former a flat interface is more likely because the flow is dominated by gravitational forces, whereas the latter tends to present a curved interface since interfacial tension also plays a role. The curvature of the interface depends on pipe geometry, physical properties of the fluids and wettability [22] and Rodriguez and Baldani [3]. The idea of a curved interface was used by Brauner et al. [23] to propose new closing equations and predict holdup and pressure drop in stratified liquid–liquid laminar flow. An experimental work was performed by Raj et al. [24] and those authors confirmed that for liquid–liquid flow the consideration of a curved interface provides better predictions, improving some correlations earlier developed based on the work of Taitel and Dukler [25] (for instance [26,27]).

An experimental work on characterization of liquid–liquid flow patterns can be seen in Trallero [26] and Trallero et al. [27], where data for horizontal flow were presented including stratified and semi-stratified flow, dispersions and emulsions. Those authors did not differentiate wavy stratified from stratified with mixing at the interface. Elseth [28] presented a more detailed horizontal oil–water flow pattern classification, observing the wavy stratified flow, and dividing Trallero's patterns into several sub-patterns. Alkaya et al. [29] continued the work of Trallero et al. [27], but now introducing the effect of pipe inclination. A wavy stratified flow pattern was reported. All the quoted authors have dealt with relatively low viscosity oils. On the other hand, Bannwart et al. [30] studied a horizontal very viscous oil–water flow and reported the stratified flow pattern among others. Interfacial waves in liquid–liquid stratified flow have been spotted, but details on the wave's geometrical properties are rarely given.

The study of wave motion is a vast scientific topic; one can cite, for instance, ocean waves in deep or shallow waters. The study of interfacial wave behavior in two-phase flow is a relatively recent research topic, but of significant importance, since key parameters as holdup and pressure drop are expected to depend on the wavy structure. In addition, an exponential increase in time or space of wave amplitude might cause instabilities and, eventually, flow pattern transition [2]. The one-dimensional two-fluid model has been suggested as a tool for analyzing separated flows [31–34] and it has been applied together with the linear hydrodynamic stability theory and the concept of an exponential increase of an interfacial perturbation wave. The study of the hydrodynamic stability of separated liquid–liquid flows, and therefore transition to dispersed flow, has been carried out by Brauner [35] and Brauner and Maron [36,37], Trallero [26], Brauner et al. [21,23], Rodriguez et al. [38] and Rodriguez and Bannwart [39]. Crowley et al. [40] studied the hydrodynamic stability of separated flows through a relation between kinematic and dynamic interfacial waves. However, those authors applied their theory for gas–liquid flow only.

There are a few studies in the literature on interfacial waves in core-annular flow. In Ooms [41], Ooms et al. [42] and Oliemans [43] it was demonstrated that the existence of waves is fundamental for the stability of the core-annular flow pattern. Feng et al. [44], working with numerical simulation, also found that waves are indispensable for the hydrodynamic stability of such liquid–liquid separated flow pattern. Soon after, several theoretical and experimental papers have been produced by the group of Joseph in which it is alleged that without the presence of waves, there is not core-annular flow [45–48]. Rodriguez and Bannwart [49] measured wave speed, amplitude and wavelength in core-annular flow

and applied the kinematic wave theory of Wallis [2] to predict the holdup of the phases with good agreement with their own experimental data. In a related paper, Rodriguez and Bannwart [50] proposed an analytical solution for the prediction of the wave geometry and compared the results with experimental data, achieving good agreement.

One might conclude that the curvature in the cross-sectional view and the longitudinal wavy structure are important for the correct modeling of the stratified liquid–liquid flow. On the other hand, information on interfacial wave properties in liquid–liquid stratified flow is scanty. Some data are presented in Al-Wahaibi and Angeli [51] and Al-Wahaibi et al. [52], but it lacks of details on wave properties. Al-Wahaibi and Angeli [53] presented a very complete study on the geometrical characteristics of the stratified oil–water flow with low viscosity oil (5.5 mPa s). Those authors connected the wave characteristics with drop formation, that the drops are formed from the increase of relative motion between the phases. A comprehensive experimental study on interfacial wave characteristic in viscous oil–water flows is presented by Castro et al. [18]. Recently, Barral and Angeli [54] working with the same fluids of Al-Wahaibi and Angeli [51] presented a study of the interface characteristics in liquid–liquid flow using a double wire conductance probe. Those authors experimentally studied the changes in stratified oil–water flows during the transition to dual continuous flow. The power spectra analysis of the probe signal showed low frequency peaks due to the pumps and high frequencies that are related to the flow transition. The measurements were done at two different points of the test line, one at the pipe inlet and other 7 m downstream. Differences in the interface were observed, e.g. the presence of large waves only at the pipe entrance. The authors were not able to find any work devoted to the systematic study of waves in stratified viscous oil–water pipe flow. Therefore, the idea of this paper is to present a more complete study on such waves, offering new experimental data on wave speed and aspect ratio (ratio between wavelength and wave amplitude), a study of the wave shape and to propose a correlation to reconstruct the interfacial wave based on a second order Fourier series, where the coefficients are given as functions of dimensionless parameters, Weber and Froude numbers. Ultimately, the dataset can be used for further numerical or theoretical investigations.

In Sections 2 and 3 the experimental setup and procedure are presented. The data processing and analysis is explained in Section 4. In Section 5 data of wavelength, amplitude and wave speed related to modified Froude and Weber numbers are offered. Section 6 presents the mean interfacial wave shape. In Section 7 a correlation for wave shape is proposed, which can be used to reconstruct the interfacial wave of viscous oil–water flow. Finally, the conclusions are drawn in Section 8.

2. Experimental setup

The experimental work was carried out at the Thermal-Fluid Engineering Laboratory of the Sao Carlos School of Engineering, USP, in a inclinable hydrophilic–oilphobic glass (borosilicate) test line (−35° to +35°) of 12 m and 0.026 m i.d. This test section has the necessary instrumentation for flow measurement with positive displacements flow meters for oil and water, thermocouples for oil temperature measurement, characterization of flow patterns by visualization, global measurements of pressure drop with differential pressure transducers and in-situ volumetric fraction by quick-closing valves technique (QCV). A schematic view of the flow loop and details related to the holdup measurement technique might be seen in Rodriguez et al. [55].

The working fluids are viscous oil and tap water. The properties of the fluids were measured at the beginning and end of the experimental campaign through proper sampling. The viscosity was measured with a rheometer Brokfield™ model LVDV-III+ with rotor SC4-18, varying the temperature with a thermostatic bath. The oil viscosity did not vary significantly from the beginning to the end of the experiments, staying on average in 0.3 Pa s at 20 °C. The oil density varied from 849 kg/m^3 to 854 kg/m^3, because of the increase of dispersed water. The interfacial tension and contact angle were measured with an optical tensiometer of KSV™ model CAM 200. The oil–water interfacial tension stayed, on average, in 0.044 N/m. The same occurred with the contact angle staying, on average, in 35° (hydrophilic–oilphobic). For the tap water it is considered that the properties did not vary.

The test section has seven transparent acrylic boxes filled with water (visualization sections) of 330 mm length and 40 mm height. They were placed at different points of the test section to allow the visualization of the flow development. The first was placed at 1.3 m from the entrance and the rest at 1.5 m apart from each other. In order to correct any remaining distortion of light due to lens and parallax effects, a correction factor was obtained for the x-coordinate and y-coordinate by inserting a ruler in the pipe filled with water. The recorded image was compared with another ruler placed outside the transparent box comparing real dimensions with dimensions from the images.

3. Experimental procedure

The oil and water flow rates would be set and after reaching steady state the flow was recorded. The injection protocol started with filling the test section with oil and leaving it for several days. Since it is an oilphobic pipe, this ensures that the pipe is wetted and has the same characteristics of a pipeline used for oil transport/production. Through a simple 45° "Y" shape junction, with no separation between the phases, at the beginning of the pipeline the fluids are injected. First the water at the desired flow rate is injected through the bottom of the junction. Then the oil is injected, and the flow is assumed developed when the oil phase reaches the end of the pipeline.

The flow was recorded by a high-speed video camera (i-SPEED 3 OLYMPUS), at a rate of 100 fps (frames per second) for 48 s at 1280 × 1024 pixels of resolution. A NIKON lens was used (focal distance of 50 mm and shuttle of f/1.4). The equipment was installed on a pedestal and two xenon lamps were used to illuminate the flow, allowing the acquisition and optical measurement of the geometrical properties and speed of the interfacial waves. The images were taken at the third transparent box, at 4.3 m from the pipe entrance. An area of the transparent box of 120 mm length by 21 mm height was selected for recording the movies, this area was delimited with black ribbons; the height is smaller than the pipe external diameter to avoid effects of light reflection at the top and bottom parts of the pipe. It was observed that all the filmed waves were in this region. A homemade LabView™-based program was used to extract the properties of the waves from the images (frames). The real-length-to-pixel conversion was achieved by using the correction factor cited in Section 2. The experiments were carried out at four different pipe inclinations: horizontal, 5° upward and downward and 10° upward. The inclinations were measured using a BOSCH™ inclination meter model DN-ML 60 with accuracy of 0.1°. In Fig. 1 one can see six snapshots of the lateral view of the oil–water flow taken with the high speed camera. The sequence starts at the top-left frame and goes to the right-down frame; the time interval between frames is of 0.01 s. The flow goes from right to left.

One can observe in the sequence of snapshots of Fig. 1 that there is more than one wave in each frame. Another conclusion taken from Fig. 1 is that the acquisition frequency is sufficient for the analyzed phenomenon.

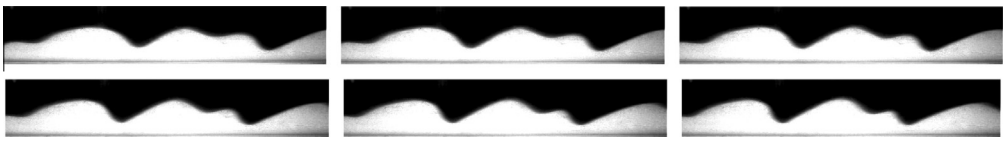

Fig. 1. Sequence of snapshots taken with the high speed camera. It starts from top-left to right-down frame; time interval between frames of 0.01 s. The flow goes from right to left, oil at the top and water at the bottom of the pipe (Uws = 0.16 m/s, Uos = 0.04 m/s, Fr^* = 0.59 and We^* = 1.31).

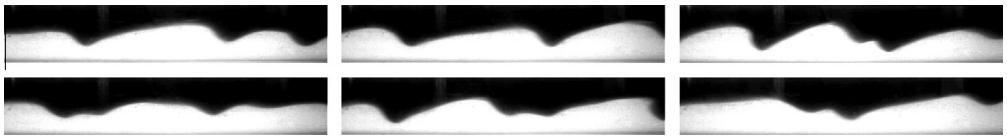

Fig. 2. Sequence of snapshots taken with the high speed camera. It starts from top-left to right-down frame; time interval between frames of 0.2 s. The flow goes from right to left, oil at the top and water at the bottom of the pipe (Uws = 0.16 m/s, Uos = 0.04 m/s, Fr^* = 0.59 and We^* = 1.31).

Fig. 2 shows six snapshots of the same flow of Fig. 1 but now with a time interval of 0.2 s. The waves have different characteristics and there are spatial and temporal changes. Notice that the wave speed may be different for each wave, which can be confirmed by the difference of the position and shape of the last two waves of frame #1 and the correspondent in frame #2 (first two waves) or in frame #3. The faster wave reaches the one that was traveling ahead, causing wave interference or superposition.

4. Data treatment and analysis

4.1. Data treatment

The software used to identify the oil–water interface and measure its amplitude (α), wavelength (λ) and speed (c) is divided in four subroutines. This is the second generation of the software presented by Castro et al. [18]. The first subroutine binarizes each frame of the film, takes off noises, cuts the ends of the images and gives the real dimensions by converting pixels to millimeters. It is important to point out that the length and height of the image are related to the pixel by a ratio of 0.093 mm/pixel (length) and 0.084 mm/pixel (height). A text file with x and y coordinates of each point of the interface in each frame is generated (Fig. 3).

The second subroutine identifies any wave present in the interface in each frame via wave-peak-and-valley search algorithm and generates a second text file with these filtered waves separated one by one. To avoid both the use of Fourier filters, which modify the wave shape, and the counting of remaining noises as interfacial waves a windowing algorithm is used, where the operator set the size of the window, and only waves bigger than this window are counted, it works as a band pass filter (Fig. 4).

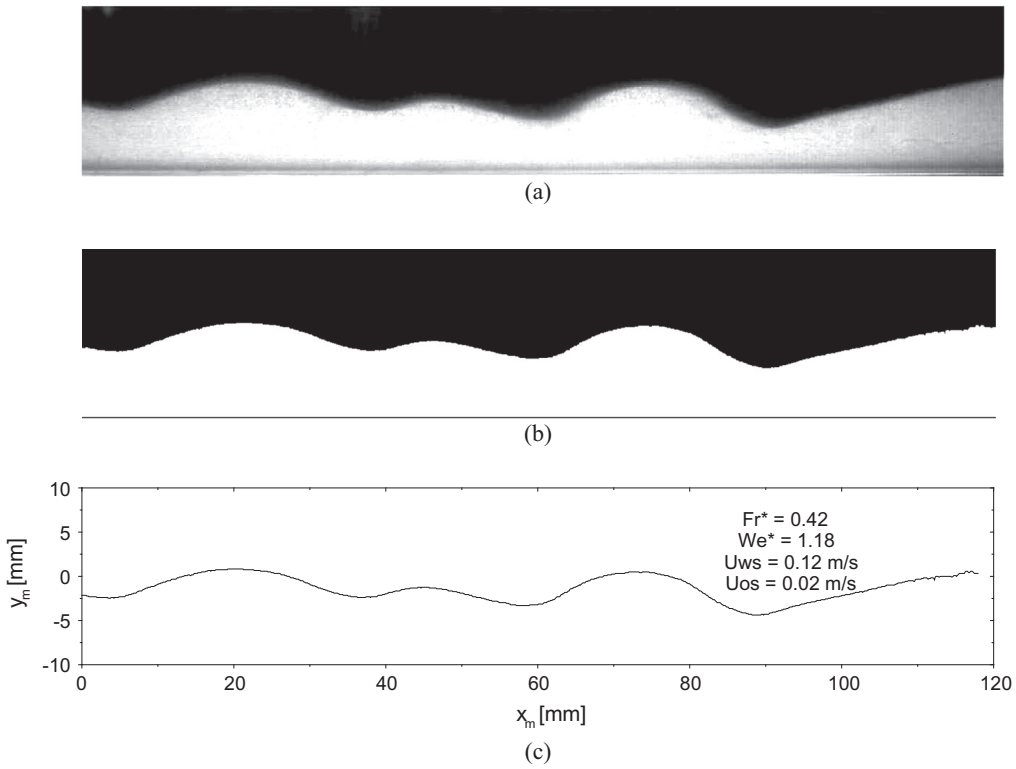

Fig. 3. (a) Real image; (b) binarized and (c) reconstruction of the image via text file (Uws = 0.12 m/s, Uos = 0.02 m/s, Fr^* = 0.42 and We^* = 1.18). Flow from right to left; oil at the top and water at the bottom.

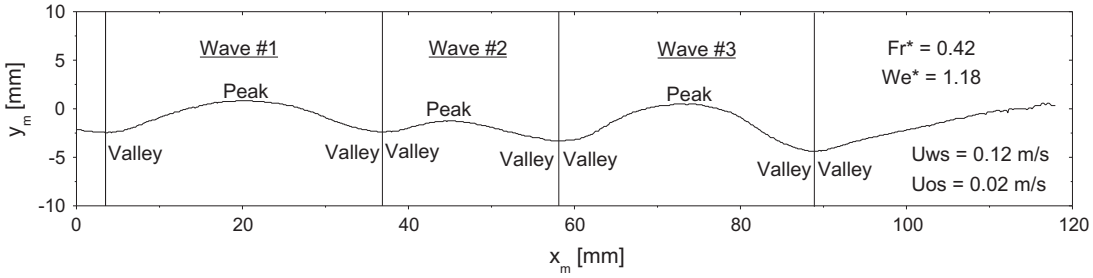

Fig. 4. Simulation of the wave-peak-and-valley search algorithm. Only three waves were separated from this frame (Uws = 0.12 m/s, Uos = 0.02 m/s, Fr^* = 0.42 and We^* = 1.18).

As the main purpose is to measure the 2-D interfacial wave, as observed in Fig. 4, only waves with a certain dimension were counted and have its dimensions measured. This also avoids any problem due to the binarization process. It should be pointed out that the procedure described above has the main purpose of keeping the wave shape information available for subsequent analysis. The third subroutine takes the new text file and calculates the wavelength (λ) and wave amplitude (α) of each wave. A PDF (probability density function) of each property is obtained and the mean values, as well as the standard deviation (S), of wavelength (λ_m) and wave amplitude (α_m) for each studied case is acquired [18].

The wave speed, (c), was calculated by 1-D cross-correlation of 4800 consecutive frames [56], with the text file given by the first routine, without any wave filtering process. The cross-correlation between two conductivity probes was used by Al-Sarkhi et al. [57] to measure the wave speed in annular gas–liquid flows.

The influence of the cross-sectional curvature of the interface on the wave properties was discussed in Castro et al. [18]. It was showed that the hypothesis of a 2-D wave, adopted in this work, is suitable, even when the cross-sectional curvature is taken into account.

4.2. Data sampling

The recording time and acquisition rate were set at 48 s and 100 fps, respectively. It was considered adequate since the maximum wave speed observed was of the order of 0.45 m/s and the test section had a length of about 4.5D (0.12 m). Therefore, in the worst case, the fastest wave crosses the visualization section in about 0.27 s and at least 27 frames are taken within this time interval.

4.3. Average wave shape

The proposed methodology to obtain the average shape of the wave was presented by Castro et al. [18]. All the waves are normalized in the x and y coordinates, by, respectively, its wavelength and pipe's internal diameter, giving the x^* and y^* normalized coordinates. The x^* coordinate varies from 0 to 1 and within this range the mean of each y^* coordinate is taken. Finally, the average wave shape is given by the x_m-coordinate and y_m-coordinate (functions of the mean wavelength, pipe's internal diameter and normalized coordinates):

$$x_m = \lambda_m \cdot x^* \tag{1}$$

$$y_m = D \cdot y^* \tag{2}$$

5. Interfacial wave properties

The water and oil superficial velocities varied from 0.05 to 0.23 m/s and 0.02 to 0.18 m/s, respectively, at several inclinations from horizontal, 0°, +5°, +10°, and −5°.

In liquid–liquid flow some relation between fluids and flow properties are observed. In the specific case of stratified flow the cross-sectional curvature and the relative velocity tend to disturb the flow, whereas gravitational and capillarity effects and viscosity of the phases are important in maintaining the flow and the interface [19,58,59]. So, the interfacial wave characteristics may be related to dimensionless numbers that include such effects. Modified Froude and Weber numbers are proposed to correlate the dimensionless wave speed and the aspect ratio of the wave, respectively. Correlations with the Reynolds numbers calculated via the hydraulic diameter and in-situ velocity [3] of each phase were also found for the wave properties.

The Froude number (Fr^*) relates a characteristic velocity to the gravitational wave velocity. In other words, it relates inertia, through the relative velocity between phases, to gravitational forces. Eq. (3) presents the proposed Froude number:

$$Fr^* = \frac{V_w - V_o}{\sqrt{g(\cos\theta) y_{car}}} \tag{3}$$

where V_w e V_o are, respectively, water and oil in-situ velocities, g is the gravity, θ is the inclination angle and y_{car} is a characteristic dimension, Eq. (4).

$$y_{car} = \varepsilon_w \frac{\pi D}{4} \tag{4}$$

where ε_w is the water holdup calculated via the 1-D two-fluid model modified by Rodriguez and Baldani [3] and D is the pipe's internal diameter.

The Weber number (We^*) represents the ratio between inertia and capillarity forces. It is often used to analyze flows where there is an interface between the phases, especially in cases where curvature is present. The proposed modified Weber number is showed in Eq. (5):

$$We^* = \frac{\Delta\rho (V_w - V_o)^2 y_{car}}{\sigma} \tag{5}$$

where $\Delta\rho$ is the difference between the density of the phases and σ is the interfacial tension between oil–water.

It is important to say that although the viscosity is not directly present in Eqs. (3)–(5), it is implicitly taken into account in the calculus of the water holdup and in-situ velocities of the phases.

The Reynolds numbers of the phases are shown in Eqs. (6) and (7):

$$Re_w = \frac{\rho_w V_w D h_w}{\mu_w} \tag{6}$$

$$Re_o = \frac{\rho_o V_o D h_o}{\mu_o} \tag{7}$$

The hydraulic diameters were calculated from the expressions proposed by Rodriguez and Baldani [3].

Table 1
Standard deviation (*S*).

Wave characteristic	Lowest *S* (%)	Highest *S* (%)	Mean *S* (%)
Wave speed	5	100	21
Wavelength	29	78	37
Wave amplitude	36	92	47

The next section shows the average characteristics of the interfacial wave as functions of the proposed Weber, Froude and Reynolds numbers.

The mean values of each wave characteristic were calculated via normal distributions (PDF) of the measurements of all the waves present in the 4800 acquired frames (14,400 waves); therefore, the standard deviation (*S*) is the parameter chosen for quantifying the error. Table 1 shows the standard deviation observed for each property.

The highest values of standard deviation are related to the smallest and slowest waves.

It is important to say that the uncertainties of the measurements are related to the capability of the program to binarize and identify the exact pixel where the valley and peak of the wave were at. As each pixel corresponds to 0.093 mm in length and 0.084 mm in height, these uncertainties are not significant.

5.1. Interfacial wave aspect ratio

The ratio between the average wavelength and average amplitude (λ_m/α_m) or interfacial wave aspect ratio is presented as a function of the Weber number for different pipe inclinations (Fig. 5). It is clear that as the relative velocity increases, the Weber number increases and the aspect ratio asymptotically decreases. In other words, the wave amplitude increases and wavelength decreases with increasing the Weber number.

Three databases were used and all have the same behavior. Therefore, it is possible to propose an exponential relation between the interfacial wave aspect ratio and the modified Weber number, as given by Eq. (8) (72% of the points are within prediction bands of ±30%):

$$\frac{\lambda_m}{\alpha_m} = 84.3e^{(-We^*/0.4)} + 6.8 \tag{8}$$

Considering the hydrodynamic stability of stratified flow, one may infer that waves with low aspect ratio represent waves on the brink of breaking up. Experimentally, Al-Wahaibi et al. [52] presented the mechanism of drop formation in stratified liquid–liquid flows. The authors concluded that the relative movement between the phases may lead to the deformation of the interfacial wave and to drops formation. The relative velocity has a destabilizing effect. As it increases it may overthrow the restoring viscous and capillarity forces, which would lead to a higher level of instability. In the cases studied in this paper, the aspect ratio of the interfacial wave decreases with increasing the relative velocity, as expected [51,52]. Flows with higher Weber numbers, over 1.1, were perceived to be near the transition from stratified wavy to stratified with mixture at the interface. It also can be inferred from Fig. 5 that the minimum stable wavelength–amplitude ratio is around 7. It is important to notice that only stable wavy stratified flows, without any drop at the interface, are presented. So, it can be concluded that flow with a Weber number higher than 1.1 and predicting wavelength–amplitude ratio lower than 7, should have already changed into stratified with mixture at the interface.

No relations between the wavelength–amplitude ratio and Froude and Reynolds numbers were observed.

Last but not least, low wavelength–amplitude ratios have been related to transition from core-annular flow to dispersed flow [39,49,50].

5.2. Interfacial wave speed

The mean interfacial wave speed is normalized by the mixture velocity (*Uws* + *Uos*) and presented as a function of Froude number (Fig. 6). The wave speed asymptotically increases with increasing the Froude number. No relation of the normalized wave speed with the Weber number was observed.

Using two databases, it is possible to propose an exponential correlation for the normalized wave speed, Eq. (9) (58% of the points are within prediction bands of ±50%, dashed lines of Fig. 6):

$$\frac{c}{(Uws + Uos)} = -2.6e^{(-Fr^*/0.4)} + 1.5 \tag{9}$$

An increase of the Froude number can be related to a higher degree of instability of the flow. It has been shown that the observed interfacial wave is kinematic in nature [59]. In accordance with the 1-D wave model for flow pattern transition [40,59], an increase of the wave speed with the Froude number

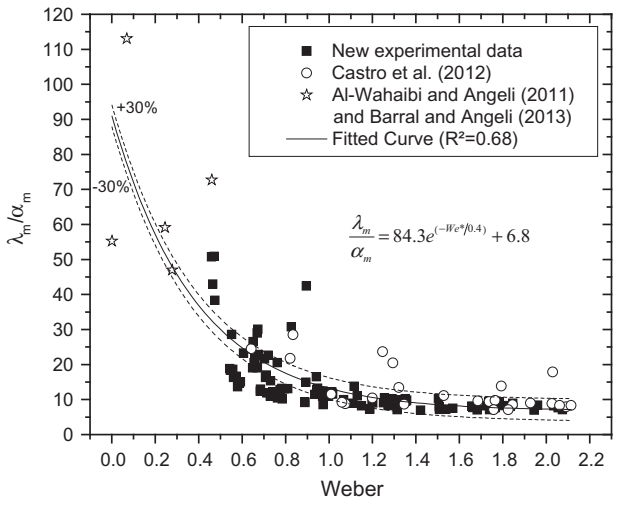

Fig. 5. Wave aspect ratio as a function of Weber number.

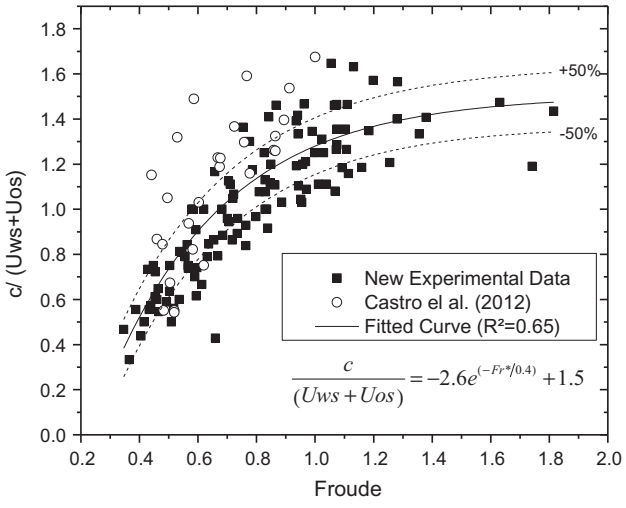

Fig. 6. Normalized wave speed as a function of the Froude number.

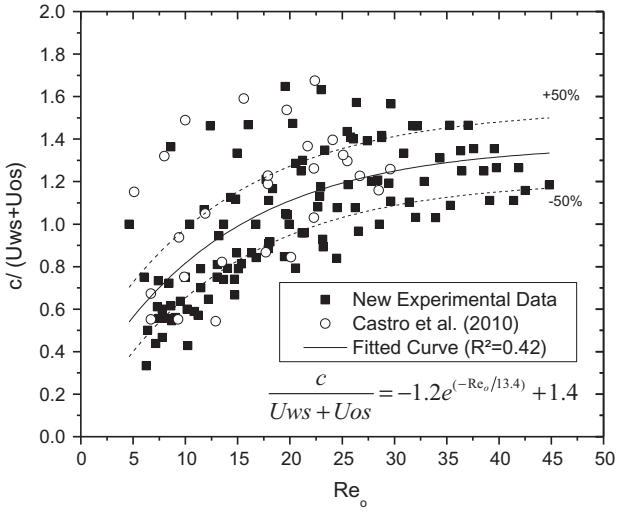

Fig. 7. Normalized wave speed as a function of the Reynolds number of oil phase.

would indicate higher trend of instability of the stratified flow pattern. In addition, according to Wallis [2], there is a limit value of the kinematic wave speed related to stable flow. One can see in Fig. 6 that the normalized wave speed presents an asymptotic curve with limit around 1.6; this value might be related to the critical wave speed proposed by Wallis [2].

It was observed that the normalized wave speed also increases with increasing the oil phase Reynolds number (Fig. 7). Only laminar oil flow was observed in this work. At this point the necessity of more experimental data is clear, especially of low viscous oil, where turbulent oil flow may be observed.

An exponential relation for the normalized wave speed, Eq. (10), is proposed using two databases (60% of the points are within are prediction bands of ±50%, dashed lines of Fig. 7):

$$\frac{c}{Uws + Uos} = -1.2e^{(Re_o/13.4)} + 1.4 \tag{10}$$

Another analysis that can be made is about the relation of the wave speed with the in-situ velocities of the phases. According to the literature, the kinematic wave speed must be in between the values of the in-situ velocities [2]. One can see in Fig. 8 three different velocities: phase's in-situ and wave speed, as functions of the mixture velocity (*Uws* + *Uos*) for all experimental points. It is observed that the interfacial wave speed is in between the other two velocities. This supports the hypothesis that the lower and upper limits of the wave speed would be the phase's in-situ velocities and that the wave is kinematic in nature; otherwise the stratified-flow stability cannot be guaranteed [2].

6. Interfacial wave shape

The average shape of the interfacial wave in stratified liquid–liquid flow seems to be still unclear. Numerical studies that simulate the propagation of interfacial waves are still based on generic waves without any connection with the physics or the intense relationship between the fluids [27,40,60,61]. It was observed that the interfacial waves resemble sea waves in the region of surfing, with steep fronts and smooth troughs, so the goal of the next sections is to provide the mean wave shape and a generic equation that can describe it. It is important to notice that in these pictures the flow occurs from right to left and that water is below and oil above the wave. Another important point is that all the waves plotted in this section are plotted with the mean value as zero, in other words, all the waves are plotted around y_m equal to zero. This was done to make the comparison easier. Notice that since the phases' superficial velocities vary, the volumetric fraction and so on the water height also vary. The water height should be the mean value of the interfacial wave. It will be the subject of study of Section 7.

6.1. Relation with flow properties

The dependence of the wave shape on the superficial velocities will be presented. Refer to Castro et al. [18] for more details on the methodology used to obtain the average wave shape.

Fig. 9 shows the variation of the wave shape with increasing the superficial velocity of water for a constant oil superficial velocity (0.1 m/s) in horizontal flow. It can be observed that as the water superficial velocity increases, the wave amplitude tends to increase as well, which indicates the typical phenomenon of steepening of short waves [62]. In addition, the waves are asymmetric with steep fronts and smooth troughs. Notice that water, which is flowing faster, is below and oil above the wave and that the flow occurs from right to left. On the windward side (right) the wave crest is gentler and it has a steeper leeward slope (left), i.e., the wave resembles an upside-down sea wave in the region where it is about to break. The Weber numbers related to the flow cases of Fig. 9 are 0.46, 0.74 and

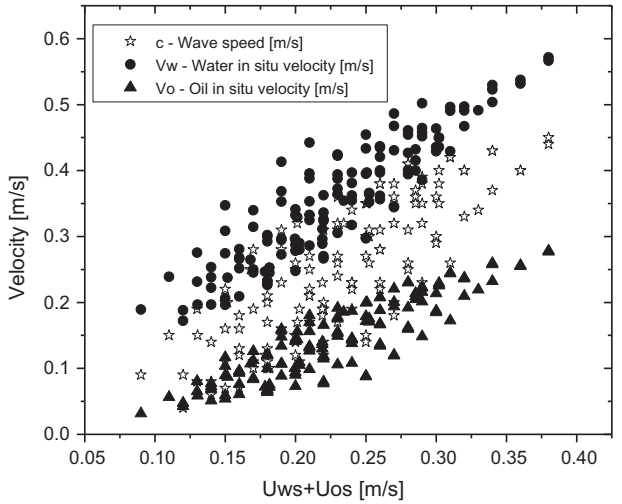

Fig. 8. Wave speed, water and oil in-situ velocities as functions of mixture velocity.

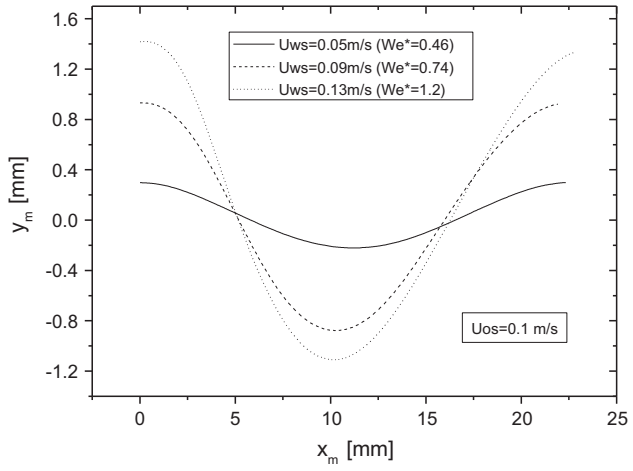

Fig. 9. Mean wave shape as a function of the water superficial velocity for a constant oil superficial velocity (0.1 m/s) in horizontal flow.

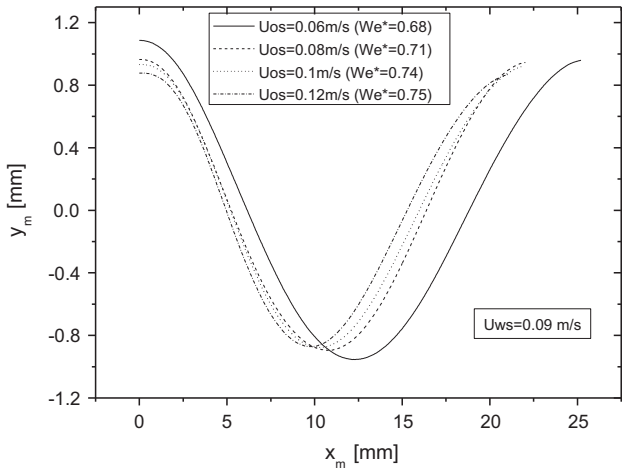

Fig. 10. Mean wave shape as a function of oil superficial velocity for a constant water superficial velocity (0.09 m/s) in horizontal flow.

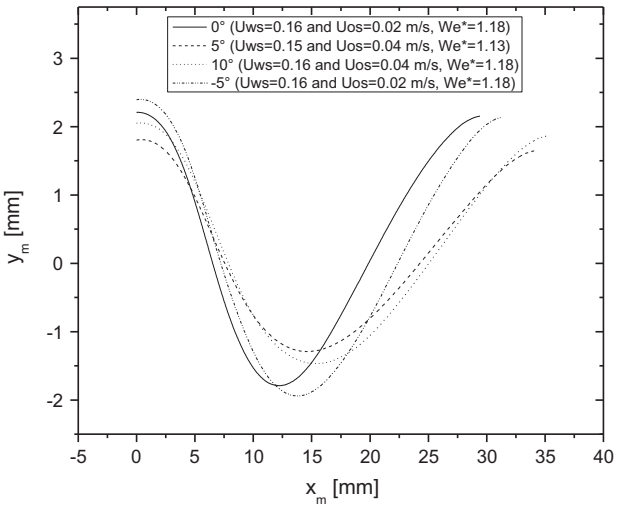

Fig. 11. Mean wave shape as a function of the pipe inclination angle (0°, 5°, 10° and −5°) for the same Weber number.

1.20. The steepening of the wave crest with increasing the Weber number was already expected (refer to Fig. 5). On the other hand, the variation of the water superficial velocity does not cause significant change on the wavelength. It seems that, for the typical case studied in this work, the wave amplitude is more sensitive to the change in the value of the water superficial velocity than the wavelength.

The dependence of the wave shape with the oil superficial velocity for constant water superficial velocity (0.09 m/s) is presented in Fig. 10. A slight decrease of the wavelength and wave amplitude with increasing the oil superficial velocity can be observed. The Weber number value related to the flow cases of Fig. 10 is almost constant and of about 0.73. In this case, an increase of the oil superficial velocity increases the relative velocity, but it decreases the water holdup. Therefore, the aspect ratio remains virtually the same (Fig. 4). One may observe once more the asymmetry of the wave.

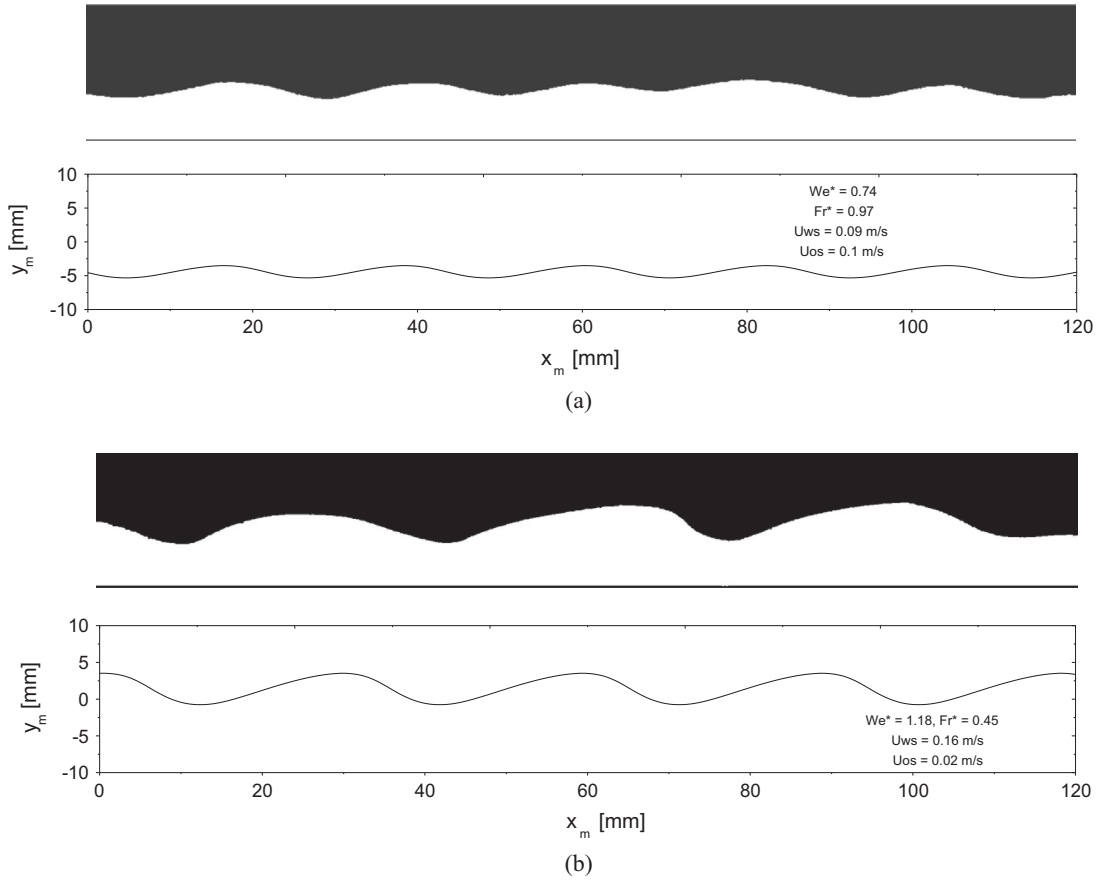

Fig. 12. Binarized wave image and reconstructed mean interfacial wave: (a) horizontal flow, *Uws* = 0.09 m/s and *Uos* = 0.1 m/s and (b) horizontal flow, *Uws* = 0.16 m/s and *Uos* = 0.02 m/s.

6.2. Relation with pipe inclination angle

As discussed in Sections 5 and 6, the aspect ratio of the waves is related to the Weber number a function of the pipe inclination (Eq. (5)) via water holdup and in-situ velocities of the phases. In Fig. 11 on can see four different waves at different pipe inclinations, but with the same (or almost) Weber number. The wave shape in upward flow (5° and 10°) is different from that in downward (−5°) or horizontal (0°) flow. In upward flow, the action of buoyancy pulls up the oil (lighter phase), which tends to flow faster, minimizing the relative velocity. The interfacial wave tends to look like a sinusoidal function. In downward flow, on the other hand, the action of gravity makes the water (heavier phase) flow faster, increasing the relative velocity. The interfacial wave resembles a sea wave in the brink of breaking up. In horizontal flow there is no direct action of buoyancy and so it is expected that the less viscous phase (water) should flow faster, as in downward flow. Again, as in downward flow, the interfacial wave tends to be as a sea wave in the surfing zone. The effect of the inclination in waves characteristics of the annular gas–liquid flow were studied by Al-Sarkhi et al. [57], and some of the conclusions reached in this work were observed by those authors, e.g. the decrease of the wave amplitude with the increase of the inclination. In that article the authors did not worked with descendent flows.

6.3. Comparison with real images

One can reconstruct the interfacial wave by sequentially assembling mean waves. These waves are compared with binarized snapshots taken from the stratified flow. Now, the mean value is added to the mean wave. Fig. 12(a) and (b) shows the binarized image and reconstructed interfacial wave with water and oil superficial velocities of 0.09 and 0.1 m/s in case (a) and of 0.16 and 0.02 m/s in case (b) horizontal flows.

In case (a) an almost sinusoidal mean wave is observed as expected looking the snapshot and the Weber number (low Weber number indicates a low amplitude high wavelength wave). In case (b), due to the difference in the Weber and Froude numbers another wave is expected, with low aspect ratio. This is what the mean wave presents, a wave resembling sea wave with high wave amplitude.

The wave-reconstruction methodology consistently captured the wave shape. The comparison with real images of the flow shows good agreement and the main qualitative wave characteristics were preserved. It is important to point out that some quantitative disagreement is expected since the reconstructed wave represents the average wave shape, whereas the binarized images are just snapshots taken from the movie with the high speed video camera.

7. Correlation for predicting the mean interfacial wave shape

A generic equation to reproduce the wavelength, wave amplitude and shape of the interfacial wave in oil–water stratified flow is an open problem. The goal of this section is to propose a correlation where the coefficients are functions of pertinent dimensionless parameters of the flow.

7.1. Correlation

Several mathematical models were attempted in order to reconstruct the observed interfacial waves. A second order Fourier series equation was the simplest and the one that gave the best results, Eq. (11):

$$y_m = A_0 + A_1\cos(wx_m) + B_1\sin(wx_m) + A_2\cos(2wx_m) + B_2\sin(2wx_m) \quad (11)$$

where y_m and x_m are the x and y-coordinates. A_0, A_1, A_2, B_1, B_2 and w are coefficients that were fit by using MatLab™ fitting tool, for each flow condition. One can see the achieved agreement in Fig. 13, where the wave predicted by Eq. (11) is compared with the experimentally obtained mean wave for several flow conditions and pipe inclinations, 0°, 5°, 10° and −5°.

It is rather clear that the proposed second order Fourier series equation fits with almost 100% of accuracy the mean interfacial wave of the flow. The mean R^2 = 0.9989 and the mean RMSE = 0.029.

The problem now is how to express the values of the coefficients of Eq. (11) in generic terms. It is suggested that these coefficients are functions of the modified Froude and Weber numbers. Increasing the order of the Fourier series only augment the number of coefficients to be adjusted and leads to a virtually zero gain in accuracy.

7.2. Coefficients of the correlation

7.2.1. Coefficient A_0

The A_0 coefficient of Eq. (8) is the mean value of the mean wave. This coefficient is the water height (h_w) parameter of the 1-D two fluid model of Rodriguez and Baldani [3], so it should be a function of several parameters of the flow, including the fluid properties and phases relative velocity. It is possible to plot this coefficient against both Weber and Froude numbers. The best correlation found was with the Froude number, presented in Fig. 14.

In the graph of Fig. 14, 60% of the points are within prediction bands of ±50%.

The linear correlation for A_0 is given by Eq. (12):

$$A_0 = -7.9Fr^* + 3.1 \quad (12)$$

Although the linear correlation is very simple, as the A_0 coefficient is the water height of the flow, it is seems very unlike that this correlation capture all the effects present in determining this flow parameter. This point has proved to be a problem of the reconstruct methodology leading to a discrepancy, not in the wave shape, but in the position, in the vertical direction, where the wave should be in the pipe. So the water height (h_w) as proposed by Rodriguez and Baldani [3], given by the two-fluid model, was used as the A_0 coefficient.

7.2.2. Coefficients A_1, B_1, A_2 and B_2

The Fourier coefficients A_1, B_1, A_2, and B_2 are the ones related to the wave amplitude and by the sum of these trigonometric functions the wave shape is achieved. The graphics of the best observed correlations with the dimensionless groups are shown in Fig. 15. The proposed correlations are given by Eqs. (13)–(16).

The linear correlation for A_1, B_1, A_2 and B_2 are given by Eqs. (13)–(16):

$$A_1 = 0.86We^* + 0.23 \quad (13)$$

$$B_1 = 0.31Fr^* - 0.4 \quad (14)$$

$$A_2 = 0.06We^* - 0.01 \quad (15)$$

$$B_2 = 0.21We^* - 0.09 \quad (16)$$

All the graphs of Fig. 15 present prediction bands of 50%. In relation to A_1 – 57% of the points are within this region; B_1 – 55%; A_2 – 55% and B_2 – 64%.

7.2.3. Coefficient w (frequency of the Fourier series)

Coefficient w is the frequency of the Fourier series related to the period of the wave and consequently to the wavelength. The wave speed is proportional to the wavelength and so on to the frequency. The speed increases with the Froude number, so it is expected that

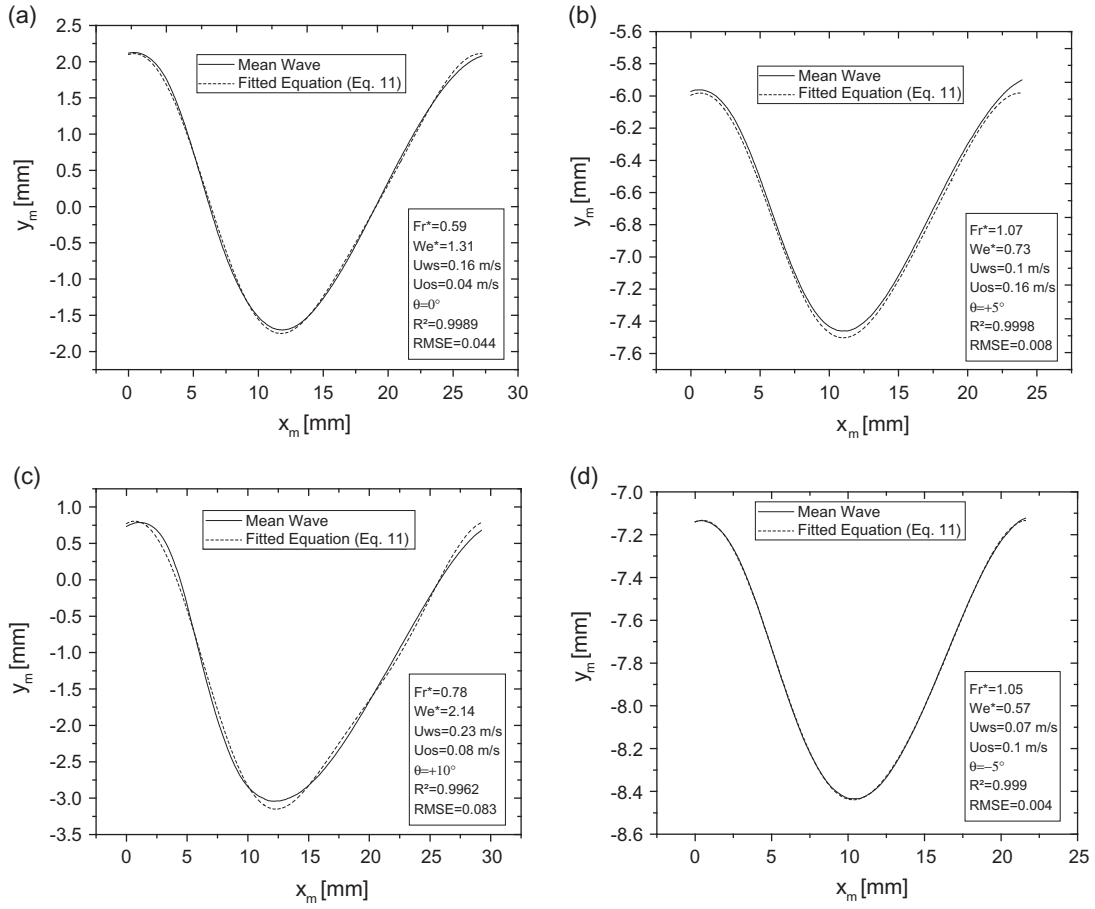

Fig. 13. Reconstructed mean interfacial waves and fitted second order Fourier series: (a) *Uws* = 0.16 m/s and *Uos* = 0.04 m/s, $\theta = 0°$; (b) *Uws* = 0.1 m/s and *Uos* = 0.16 m/s, $\theta = +5°$; (c) *Uws* = 0.23 m/s and *Uos* = 0.08 m/s, $\theta = +10°$ and (d) *Uws* = 0.07 m/s and *Uos* = 0.1 m/s, $\theta = -5°$.

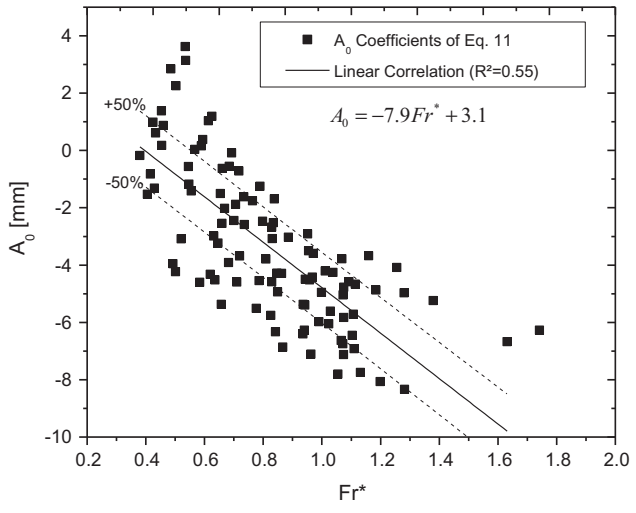

Fig. 14. A_0 coefficient against the modified Froude number, black line is a linear correlation.

the same occurs with the frequency. Hence, one can see in Fig. 16 the correlation of frequency *w* with the Froude number, where the frequency increases with the Froude number as expected. No clear correlation was observed with the modified Weber number. In relation to the correlation, 65% of the points are within prediction bands of 50%.

The linear correlation for *w* is given by Eq. (17):

$$w = 0.17Fr^* + 0.09 \tag{17}$$

7.2.4. Generic correlation for the mean wave shape

The generic correlation to reconstruct the interfacial wave of the typical viscous oil–water stratified flow of this work is given by Eq. (18) with A_0 as a function of the Froude number or A_0 as the water height. In this article the water height will be used because of the reasons mentioned in Section 7.2.1.

$$y_m = h_w + A_1(We^*)\cos[w(Fr)x_m] + B_1(Fr^*)\sin[w(Fr)x_m] + A_2(We^*)\cos[2w(Fr)x]x_m + B_2(We)\sin[2w(Fr)x_m] \tag{18}$$

7.3. Predictions

As the modified Weber and Froude numbers are known quantities and the water height might be calculated from the two-fluid model [3], it is possible to predict the interfacial wave shape by applying the proposed correlation (Eq. (18)), with the coefficients given by the relations of Eqs. (13)–(17). Some reconstructions are shown in Fig. 17 for different pipe inclinations and flow conditions.

Fig. 17(a) and (b) shows the predicted and experimentally obtained mean wave for horizontal flow, respectively, with low and high Weber numbers, the agreement is quite good in both cases. In case (a) both waves have the same shape, wave amplitude and a difference of 5 mm (22%) in the wavelength and 0.6 mm (13%) in the mean value. In case (b) both waves have almost the same shape and a difference of 0.6 mm (30%) in the wave ampli-

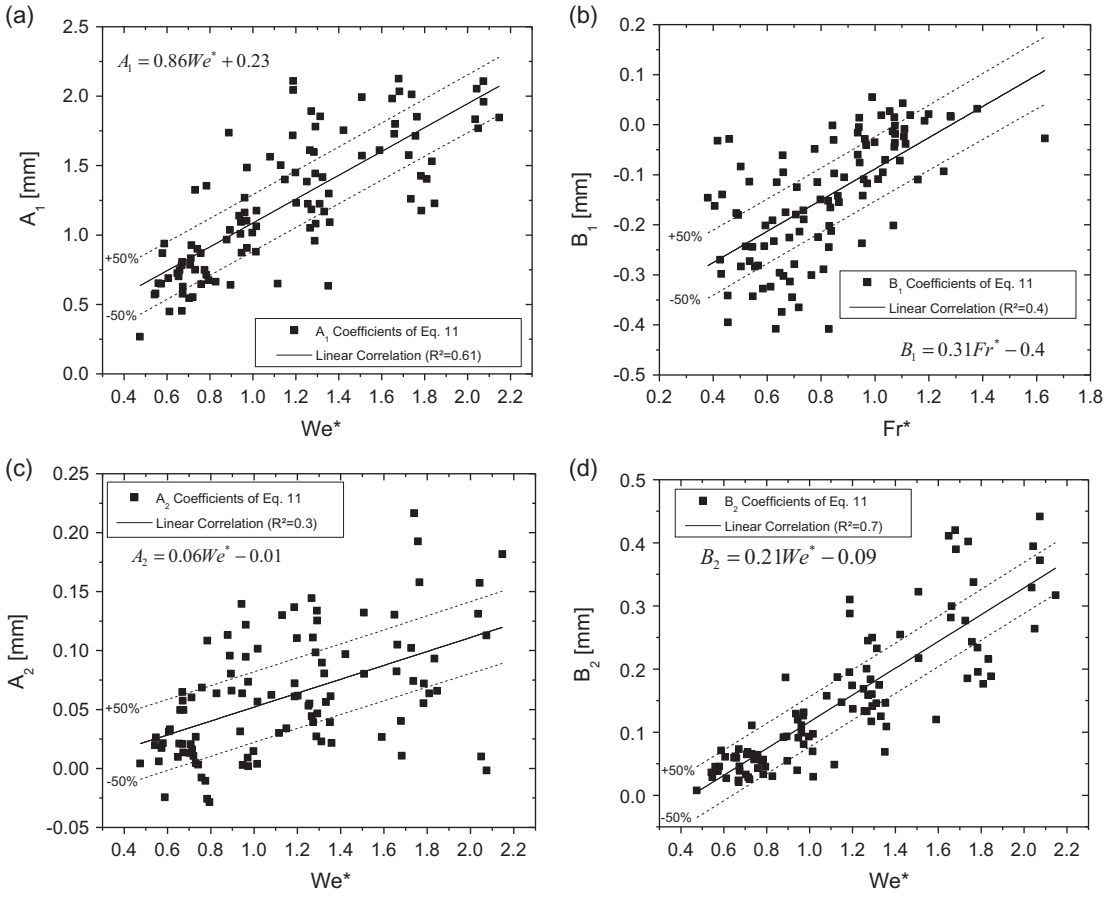

Fig. 15. Coefficients against modified Weber and Froude numbers: (a) A_1 (Weber); (b) B_1 (Froude); (c) A_2 (Weber) and (d) B_2 (Weber). Black lines are linear correlation for the points and dashed lines are prediction band of 50%.

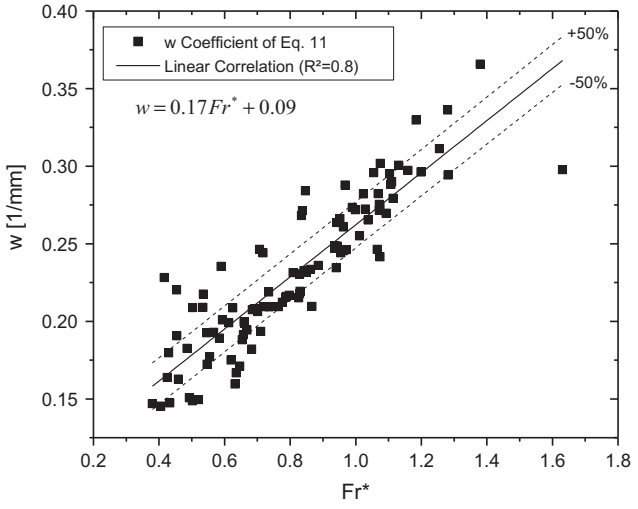

Fig. 16. *w* coefficient against the modified Froude number, black line is a linear correlation for the points, dashed lines are prediction bands of 50% (65% of the points are within these bands).

tude, 1 mm (5%) in the wavelength and 0.5 mm (12%) in the mean value.

Fig. 17(c) and (d) also presents predicted and experimentally mean waves, but now at 5° upward flow. Fig. 17(c) presents a low Weber number flow, it can be seen that the waves have the same shape and wavelength, but as well as in the horizontal case, difference in the mean value of 1.6 mm (35%). Almost all the same conclusions can be drawn about Fig. 17(d), the same shape, same wavelength, difference of 0.2 mm (7%) in the wave amplitude, and difference of 1.6 mm (35%) in the mean value.

Fig. 17(e) and (f) presents the waves for 10° upward flow, again, for low and high Weber numbers respectively. In all cases the shape of the predicted and experimental wave are the same. In the low Weber case (Fig. 17(e)) the waves have the same amplitude, difference of 0.6 mm (2.1%) in the wavelength, and 2.1 mm (45%) in the mean wave value. In the high Weber number case (Fig. 17(f)), difference of 0.35 mm (14%) in the wave amplitude, 1.4 mm (6%) in the wavelength and 1.84 mm (37%) in the wave mean value.

In 5° downward flow, only cases of low Weber number were seen, and in the plotted case the wave shape, wave amplitude and wavelength are the same and a difference of 1.1 mm (14%) in the mean value is observed.

It can be observed that in all cases the wave shape seems to be captured with good accuracy, so the main goal of the methodology was achieved (Fig. 17). Also, in almost all cases the wave amplitude and wavelength were predicted with a low uncertainty, but it is clear that more experimental data, that did not exist in the literature, are necessary to improve the quality of the correlations used in Eq. (18) and so on, the accuracy of wavelength and wave amplitude predictions.

Only for the horizontal cases the use of the water height as the mean value for locating the position of the wave predicted a wave below the experimental wave, but with a low error. For the other pipe inclinations, waves above the experimental ones were pre-

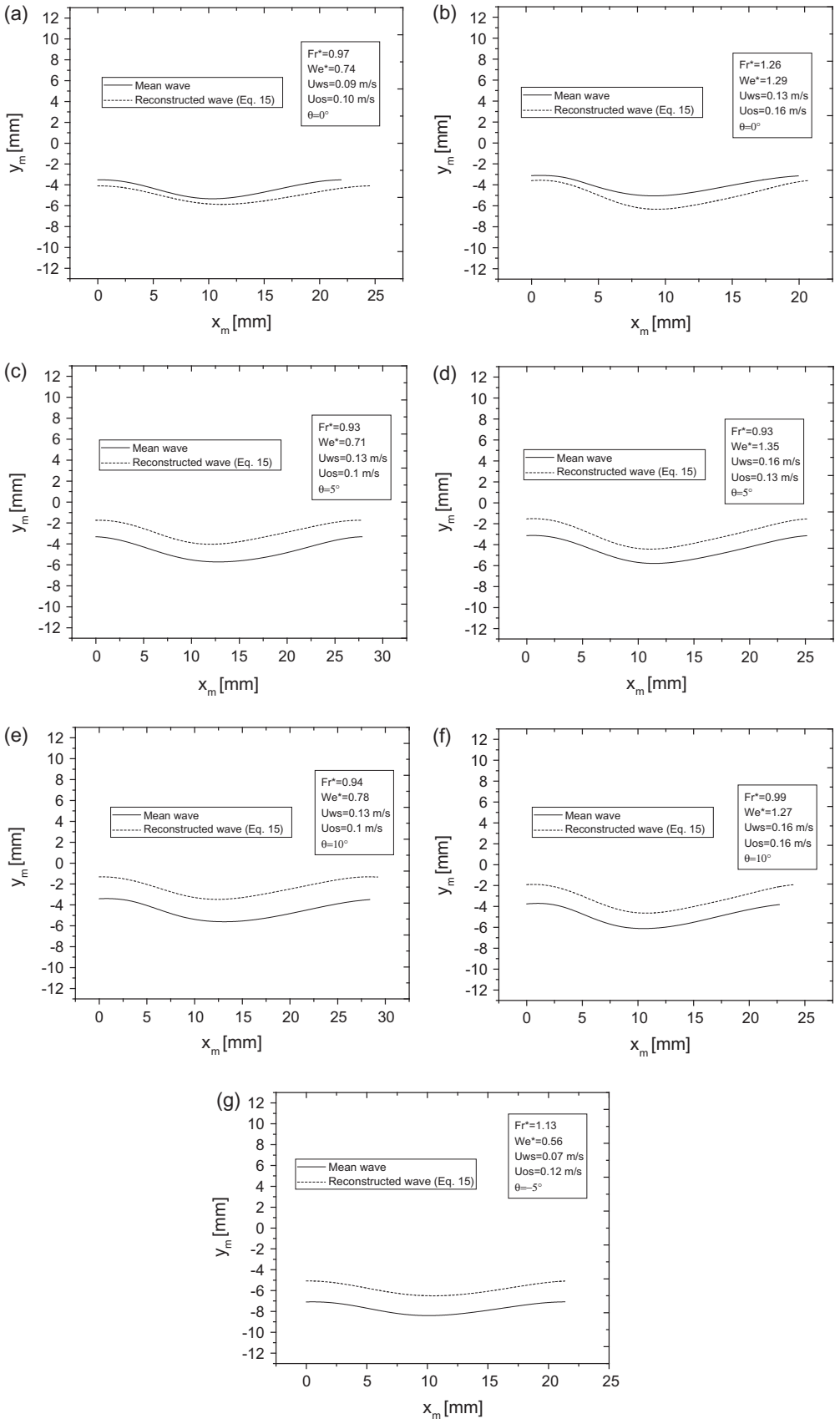

Fig. 17. Mean and reconstructed (Eq. (18)) waves: (a) low Weber number, horizontal flow; (b) high Weber number, horizontal flow; (c) low Weber number, 5° upward flow; (d) high Weber number, 5° upward flow; (e) low Weber number, 10° upward flow; (f) high Weber number, 10° upward flow and (g) low Weber number, 5° downward flow.

dicted and with relatively higher errors. However, one should notice that the maximum difference observed in the wave position was of 2.1 mm, which is lower than 10% of the pipe's internal diameter. In cases (a) and (b) of Fig. 17 the difference in the wave position is related to a difference of 10% in the water volumetric fraction, and in the others cases this difference ranged from 21% to 26%. The average deviation of holdup predicted by the two-fluid model of Rodriguez and Baldani [3] with experimental data was of 13%, with a maximum of 26%, which is in fair agreement with the presented data. It can be inferred that the errors in locating the position of the interface are due to the application of the chosen two-fluid model [3] and are independent of the methodology's capability of predicting with good accuracy the average wave shape, wave amplitude and wavelength.

8. Conclusions

An experimental study that focused on the interfacial wave observed in stratified viscous oil–water flow was conducted. The collected data on wave amplitude, wavelength and wave speed were found to be dependent on holdup, pipe inclination, relative velocity, interfacial tension and density of the liquid phases. Modified Weber and Froude numbers are proposed and used to correlate the wave aspect ratio and dimensionless wave speed. A correlation of the dimensionless wave speed with the Reynolds number of the oil phase was also observed. High Weber numbers were related in this work to steeper waves, i.e., to high-amplitude and short-wavelength waves, which are those usually observed in studies of hydrodynamic instability and flow pattern transition. The dimensionless wave speed was given as a function of the Froude number; the higher Froude number, the faster the wave speed. The proposed correlations can be used to predict with good accuracy the geometric and kinematic properties of the typical interfacial waves observed in this work.

The average wave shape experimentally obtained resembles a sea wave in the region where it is about to break. A correlation is given in order to reconstruct the typical interfacial waves observed in stratified oil–water flow. It is based on a second order Fourier equation, where the coefficients are the water height, given by the 1-D two-fluid model, and linear functions related to the proposed Froude and Weber numbers. The proposed methodology allowed for the fair prediction of the average wave shape, wavelength and wave amplitude.

Acknowledgments

The authors are grateful to FAPESP (Fundação de Amparo à Pesquisa do Estado de São Paulo, process 2010/03254-5) and PETROBRAS (Petróleo Brasileiro S. A.) for the financial support.

References

[1] D.P. Frisk, J. Davis, The enhancement of heat transfer by waves in stratified gas–liquid flow, Int. J. Heat Mass Transfer 15 (1972) 1537–1552.
[2] G.B. Wallis, One Dimension Two-phase Flow, first ed., McGraw-Hill, New York, 1969.
[3] O.M.H. Rodriguez, L.S. Baldani, Prediction of pressure gradient and holdup in wavy stratified liquid–liquid pipe flow, J. Petrol. Sci. Eng. 96–97 (2012) 140–151.
[4] V. Bontozoglou, T.J. Hanratty, Wave height estimation in stratified gas–liquid flows, AIChE J. 35 (1989) 1346–1350.
[5] V. Bontozoglou, Weakly nonlinear Kelvin-Helmholtz waves between fluids of finite depth, Int. J. Multiph. Flow 17 (1991) 509–518.
[6] G.J. Li, L. Guo, X.J. Chen, An experimental investigation on the interfacial waves in air–water two-phase flow within horizontal pipelines, Chin. J. Chem. Eng. 5 (1997) 316–324.
[7] C. Tzoti, N. Andritsos, Interfacial shear stress in wavy stratified gas–liquid flow in horizontal pipes, Int. J. Multiph. Flow 54 (2013) 43–54.
[8] Z.L. Wang, K.S. Gabriel, D.L. Manz, The influences of wave height on the interfacial friction in annular gas–liquid flow under normal and microgravity conditions, Int. J. Multiph. Flow 30 (2004) 1193–1211.
[9] Z.L. Wang, K.S. Gabriel, Z.F. Zhu, The effects of gravity on the features of the interfacial waves in annular two-phase flow, Micrograv. Sci. Technol. 15 (2004) 19–27.
[10] A. Dyment, A. Boudlal, A theoretical model for gas–liquid slug flow in down inclined ducts, Int. J. Multiph. Flow 30 (2004) 512–550.
[11] P.A. Berthelsen, T. Ytrehus, Calculations of stratified wavy two-phase flow in pipes, Int. J. Multiph. Flow 31 (2005) 571–592.
[12] N. Andritsos, T.J. Hanratty, Influence of interfacial waves in stratified gas–liquid flows, AIChE J. 33 (3) (1987) 444–454.
[13] N. Andritsos, T.J. Hanratty, Interfacial instabilities for horizontal gas–liquid flows in pipelines, Int. J. Multiph. Flow 13 (5) (1987) 583–603.
[14] N. Andritsos, Statistical analysis of waves in horizontal gas–liquid flow, Int. J. Multiph. Flow 18 (3) (1992) 465–470.
[15] D.P. Chakrabarti, G. Das, S. Ray, Pressure drop in liquid–liquid two phase horizontal flow: experiment and prediction, Chem. Eng. Technol. 28 (9) (2005) 1003–1009.
[16] D.P. Chakrabarti, G. Das, P.K. Das, Identification of stratified liquid–liquid flow through horizontal pipes by a non-intrusive optical probe, Chem. Eng. Sci. 62 (2007) 1861–1876.
[17] M.E. Charles, L.U. Lilleleht, An experimental investigation of stability and interfacial waves in co-current flow of two liquids, J. Fluid Mech. 22 (2) (1965) 217–224.
[18] M.S. Castro, C.C. Pereira, J.N. Santos, O.M.H. Rodriguez, Geometrical and kinematic properties of interfacial waves in stratified oil water flow in inclined pipe, Exp. Therm. Fluid Sci. 37 (2012) 171–178.
[19] G. Sotgia, P. Tartarini, E. Stalio, Experimental analysis of flow regimes and pressure drop reduction in oil–water mixtures, Int. J. Multiph. Flow 34 (2008) 1161–1174.
[20] N. Yusuf et al., Effect of oil viscosity on the flow structure and pressure gradient in horizontal oil–water flow, Chem. Eng. Res. Des. 90 (2012) 1019–1030.
[21] N. Brauner, J. Rovinsky, D.M. Maron, Determination of the interface curvature in stratified two-phase systems by energy considerations, Int. J. Multiph. Flow 22 (1996) 1167–1185.
[22] T.S. Ng, C.J. Lawrence, G.F. Hewitt, Interface shapes for two-phase laminar stratified flow in a circular pipe, Int. J. Multiph. Flow 27 (2001) 1301–1311.
[23] N. Brauner, D.M. Maron, J. Rovinsky, A two-fluid model for stratified flows with curved interfaces, Int. J. Multiph. Flow 24 (1989) 975–1004.
[24] T.S. Raj, D.P. Chakrabarti, G. Das, Liquid–liquid stratified flow through horizontal conduits, Chem. Eng. Technol. 28 (2005) 899–907.
[25] Y. Taitel, A.E. Dukler, A model for predicting flow regime transitions in horizontal and near horizontal gas–liquid flows, AIChE J. 22 (1976) 47–55.
[26] J.L. Trallero, Oil–water Flow Patterns in Horizontal Pipes, Dissertation, University of Tulsa, Tulsa, 1995.
[27] J.L. Trallero, C. Sarica, J.P. Brill, A study of oil/water flow patterns in horizontal pipes, SPE Prod. Facil. 12 (1997) 165–172.
[28] G. Elseth, An Experimental Study of Oil–water Flow in Horizontal Pipes, Dissertation, Norwegian University of Science and Technology, Trodheim, 2001.
[29] B. Alkaya, S.S. Jayawardena, J.P. Brill, Oil–water flow patterns in slightly inclined pipes, in: Proceeding of ETCE/OMAE2000 International Conference of Energy for the New Millennium, New Orleans, ASME, New York, 2000, pp. 14–17.
[30] A.C. Bannwart et al., Flow patterns in heavy crude oil–water flow, J. Energy Resour. Technol. 126 (2004) 184–189.
[31] K.H. Ardron, One-dimensional two-fluid equations for horizontal stratified two-phase flow, Int. J. Multiph. Flow 6 (1980) 295–304.
[32] A.V. Jones, A. Prosperetti, On the suitability of first-order differential models for two-phase flow prediction, Int. J. Multiph. Flow 11 (1985) 133–148.
[33] A.V. Jones, A. Prosperetti, The linear stability of general two-phase flow models – II, Int. J. Multiph. Flow 13 (1987) 161–171.
[34] J.H. Song, M. Ishii, On the stability of a one-dimensional two-fluid model, Nucl. Eng. Des. 204 (2001) 101–115.
[35] N. Brauner, Two-phase liquid–liquid annular flow, Int. J. Multiph. Flow 17 (1991) 59–76.
[36] N. Brauner, D.M. Maron, Stability analysis of stratified liquid–liquid flow, Int. J. Multiph. Flow 18 (1992) 103–121.
[37] N. Brauner, D.M. Maron, Flow pattern transitions in two-phase liquid–liquid flow in horizontal tubes, Int. J. Multiph. Flow 18 (1992) 123–140.
[38] O.M.H. Rodriguez, R.V.A. Oliemans, R.F. Mude, Stability analysis of slightly-inclined stratified oil–water flow, including the distribution coefficients and the cross-section curvature, in: Proceedings of 5th North American Conference Multiphase Technol., Banff, 2006, pp. 229–245.
[39] O.M.H. Rodriguez, A.C. Banwart, Stability analysis of core-annular flow and neutral stability wave number, AIChE J. 54 (2008) 20–31.
[40] C.J. Crowley, G.B. Wallis, J.J. Barry, Validation of a one-dimensional wave model for the stratified-to-slug flow regime transition, with consequences for wave growth and slug frequency, Int. J. Multiph. Flow 18 (1992) 249–271.
[41] G. Ooms, The hydrodynamic stability of core-annular flow of two ideal liquid, Appl. Sci. Res. (1972), http://dx.doi.org/10.1007/bf01897844.
[42] G. Ooms, A. Seagal, A.J. Van Der Wees, R. Meerhoff, R.V.A. Oliemans, A theoretical model for core annular flow of a very viscous oil core and a water annulus through a horizontal pipe, Int. J. Multiph. Flow 10 (1984) 41–60.

[43] R.V.A. Oliemans, The Lubricating-film Model for Core-annular Flow, Dissertation, Technische Hogeschool Delft, Delft University, Delft, 1986.
[44] Feng, P.Y. Huang, D.D. Joseph, Dynamic simulation of the motion of capsules in pipelines, J. Fluid Mech. 286 (1995) 201–227.
[45] A. Huang, D.D. Joseph, Stability of eccentric core annular flow, J. Fluid Mech. 282 (1995) 233–245.
[46] H.H. Hu, N. Patankar, Non-axisymmetric instability of core-annular flow, J. Fluid Mech. 290 (1995) 213–224.
[47] Bai, K. Kelkar, D.D. Joseph, Direct simulation of interfacial waves in a high viscosity ratio and axisymmetric core annular flow, J. Fluid Mech. 32 (1996) 1–34.
[48] R. Bai, D.D. Joseph, Steady flow and interfacial shapes of a highly viscous dispersed phase, Int. J. Multiph. Flow 26 (2000) 1469–1491.
[49] O.M.H. Rodriguez, A.C. Banwart, Experimental study on interfacial waves in vertical core flow, J. Petrol. Sci. Eng. 54 (2006) 140–148.
[50] O.M.H. Rodriguez, M.S. Castro, Interfacial-tension-force model for the wavy-stratified liquid–liquid flow pattern transition, Int. J. Multiph. Flow 58 (2014) 114–126.
[51] T. Al-Wahaibi, P. Angeli, Transition between stratified and non-stratified horizontal oil–water flows. Part I: stability analysis, Chem. Eng. Sci. 62 (2007) 2915–2928.
[52] T. Al-Wahaibi, M. Smith, P. Angeli, Transition between stratified and non-stratified horizontal oil–water flows. Part II: mechanism of drop formation, Chem. Eng. Sci. 62 (2007) 2929–2940.
[53] T. Al-Wahaibi, P. Angeli, Experimental study on interfacial waves in stratified horizontal oil–water flow, Int. J. Multiph. Flow 37 (2011) 930–940.
[54] A.H. Barral, P. Angeli, Interfacial characteristics of stratified liquid–liquid flows using a conductance probe, Exp. Fluids 54 (1604) (2013).
[55] I.H. Rodriguez, H.K.B. Yamaguti, M.S. Castro, M.J. Da Silva, O.M.H. Rodriguez, Slip ratio in dispersed viscous oil–water pipe flow, Exp. Therm. Fluid Sci. 35 (2011) 11–19.
[56] J.S. Bendat, A.G. Piersol, Random Data: Analysis and Measurement Procedures, John Wiley & Sons, New York, 2000.
[57] A. Al-Sarkhi, C. Sarica, K. Magrini, Inclination effects on wave characteristics in anular gas–liquid flows, AIChE J. 58 (4) (2012) 1018–1029, http://dx.doi.org/10.1002/aic.12653.
[58] M.S. Arney, R. Bai, E. Guevara, D.D. Joseph, K. Liu, Friction factor and holdup studies for lubricated pipeling – I, Int. J. Multiph. Flow 19 (6) (1993) 1061–1076.
[59] O.M.H. Rodriguez, M.S. Castro, Interfacial-tension-force model for the wavy-stratified liquid–liquid flow pattern transition, Int. J. Multiph. Flow 58 (2014) 114–126.
[60] D. Barnea, Y. Taitel, Non-linear interfacial instability of separated flows, Chem. Eng. Sci. 49 (1994) 2341–2349.
[61] Y. Salhi, E. Si-Ahmed, J. Legrand, G. Degrez, Stability analysis of inclined stratified two-phase gas–liquid flow, Nucl. Eng. Des. 240 (2010) 1083–1086.
[62] M.L. Banner, W.K. Melville, On the separation of air flow over water waves, J. Fluid Mech. 77 (1976) 825–842.